Article

Stochastic Expansion Planning of Various Energy Storage Technologies in Active Power Distribution Networks

Reza Sabzehgar [1,*] , Diba Zia Amirhosseini [1], Saeed D. Manshadi [1] and Poria Fajri [2]

1   Department of Electrical and Computer Engineering, San Diego State University, San Diego, CA 92182, USA; dziaamirhosseini@sdsu.edu (D.Z.A.); smanshadi@sdsu.edu (S.D.M.)
2   Department of Electrical and Biomedical Engineering, University of Nevada Reno, Reno, NV 89557, USA; pfajri@unr.edu
*   Correspondence: rsabzehgar@sdsu.edu; Tel.: +1-619-594-7791

Abstract: This work aims to minimize the cost of installing renewable energy resources (photovoltaic systems) as well as energy storage systems (batteries), in addition to the cost of operation over a period of 20 years, which will include the cost of operating the power grid and the charging and discharging of the batteries. To this end, we propose a long-term planning optimization and expansion framework for a smart distribution network. A second order cone programming (SOCP) algorithm is utilized in this work to model the power flow equations. The minimization is computed in accordance to the years (y), seasons (s), days of the week (d), time of the day (t), and different scenarios based on the usage of energy and its production (c). An IEEE 33-bus balanced distribution test bench is utilized to evaluate the performance, effectiveness, and reliability of the proposed optimization and forecasting model. The numerical studies are conducted on two of the highest performing batteries in the current market, i.e., Lithium-ion (Li-ion) and redox flow batteries (RFBs). In addition, the pros and cons of distributed Li-ion batteries are compared with centralized RFBs. The results are presented to showcase the economic profits of utilizing these battery technologies.

Keywords: battery energy storage system (BESS); lithium-ion battery; redox flow battery (RFB); stochastic expansion planning; second order cone programming (SOCP); power optimization; power distribution network; smart distribution network

1. Introduction

In today's world, many technologies and technological devices that are used on a daily basis, whether it is for personal or commercial use, rely on fossil fuels as their generation source of electricity. This dependence has led to an increase in the greenhouse gas (GHG) emissions, as well as other related fossil fuel pollution in the environment, and stirred an interest in utilizing renewable energy resources [1,2]. Renewable energy resources, such as wind turbines, solar panels, and hydro-power are freely available, pollution free, and durable, which are the main reasons for growing industrial and residential interest in utilizing these resources. This has therefore led to the transformation of these units into smart microgrids [1,3]. Smart microgrids use wireless networks for energy data collection, power line monitoring, protection, and demand/response management, and have made energy usage more flexible and economically efficient [4]. Smart microgrids, however, are dependent on renewable energy resources, and these resources are considered to be unreliable due to their stochastic behavior and their dependency on factors such as weather, wind speed, cloud cover, humidity, elevation, and solar irradiance. There are periods of time when these resources might not be able to provide any energy to support the microgrid, which is the reason why energy storage systems (ESS) are integrated into the microgrids [5]. Consequently, one of the priorities of the Department of Energy (DOE) [6] for smart grid development is the integration of appropriate batteries and other storage

systems. ESS can help with frequency and voltage regulation, capacity support, reactive power compensation, and peak shaving [7–10].

Many countries including the Unites States have adopted, funded, and supported ESS projects; however, many industries are interested in a technology that can be sustainable and independently-operated. The fact that needs to be addressed is that once this technology becomes independently-owned, it has to participate in the electricity market, which could eventually lead to increasing costs for the customers. Hence, it is of the utmost importance to adopt a technology and battery chemistry that is economically beneficial to the customers in the long term [11].

To address these concerns, several research studies have been conducted that focus on finding the best battery technologies that could be used for electrochemical energy storage applications. Among all battery technologies, Lithium-ion (Li-ion) battery technology has evolved over 40 years and proven itself as the dominant battery technology powering up everything from small electronic devices, to rechargeable energy resources in electric vehicles, and to energy storage systems in residential units [12,13]. Li-ion batteries are very lightweight compared to other batteries, allowing them to have a very high energy density. Despite the advantages and domination of Li-ion battery technology in current battery storage market, it does not provide the needed solution for the utility-scale commercial battery market due to its short operating life and its issues with rapid heat generation. A majority of grid storage today is pumped hydro, but there are geologic and environmental constraints on the deployment location of pumped hydro. Therefore, utility grids need large-scale, stable, and long-lasting chemical battery storage to deal with rapid intermittency of renewable energy generation resources and fast load changes. Vanadium redox flow battery (RFB) technology offers several advantages such as scalability, non-flammability, compactness, low maintenance, long life cycle, high efficiency, high charge and discharge duration, durability, and fast responsiveness [14,15]. Furthermore, the Earth's crust has more vanadium than lithium. However, the commercialization of RFB technology suffers from the high cost of Vanadium extraction, which is why RFB technology has only been utilized in the industry and it is not currently economically viable for residential and home storage applications [16].

There are several works in the literature that have compared the performance of Li-ion batteries [17] with RFBs and have studied their effects on the grid and users [18,19]. In [20], a comprehensive assessment of a prospective production process for RFBs is presented showing that compared to Li-ion batteries, RFBs exhibit lower costs of manufacturing, due to their simpler reactor (cell) design, lower required area, and thus a simpler manufacturing process. It is also shown that RFBs, compared to competitive technologies such as Li-ion batteries, are projected to achieve the majority of manufacturing scale benefits at lower production volumes, but this advantage is offset due to the remarkably lower current production volume of flow batteries. In [21,22], novel strategies are presented to achieve the goal of high energy density for RFBs and to address one of the inhibiting factors in widespread utilization of RFBs in utility-scale energy storage systems. A comprehensive review of RFBs and their potentials as future utility-scale battery storage systems is presented in [23,24]. In [25,26], it is demonstrated that utilizing batteries and storage systems will improve the efficiency and reliability of the grid. Other studies have focused on combined utilization of batteries and renewable energy sources in order to compensate for the stochastic characteristics of these resources and to help utility companies with peak shaving [27–29]. However, none of the available articles have addressed how the installation, operation, and maintenance costs of each of these batteries might affect the utility's and customer's decision in adopting these battery technologies.

Therefore, to outline the potential benefits of RFBs in meeting stringent cost target for grid applications and to shed some light on the viability of RFB technology as a promising solution for future utility-scale battery storage system, we have investigated the optimal cost and the benefits of deploying RFB technology and compared it with the current mature and dominant Li-ion battery storage technology. Comparison of RFB, as

a centralized battery technology, and Li-ion battery, as a decentralized technology, also reveals the impacts and economic profits of these two battery technologies. To this end, this work proposes a long term planning optimization and expansion framework for a smart distribution network having combined centralized battery technology, e.g., RFB and decentralized technology, e.g., Li-ion battery as well as renewable energy resources, such that the grid would have optimal power flow with AC power flow constraints. A second order cone programming (SOCP) algorithm is utilized in this work to model the power flow equations [30–32]. Leveraging the full AC power flow constraints enables an accurate modeling for the loss as well as voltage drop across the distribution network. One major research question analyzed in this work is the impact of the location of the storage units as well as the size and the procured technologies. The full AC power flow constraints embedded into the long-term expansion planning framework ensure that all operating conditions are satisfied. The presented analysis reveals the impact of each type of technology on both economics of the system as well as operating criteria. This work will pave the way toward a wise decision in choosing and deployment of a proper battery technology among various technologies. The contribution and objective of this work is to minimize the cost of installing renewable energy resources as well as energy storage systems (batteries), in addition to the cost of operation over a period of 20 years, which will include the cost of operating the grid as well as the charging and discharging of the batteries. The numerical results are presented to showcase the economic profits of operating investor-owned batteries (Li-ion battery in this case) and utility-owned battery storage systems (RFB in this case). The highlights of this work can be summarized as follows:

- In this work, a long-term planning optimization and expansion framework for a smart microgrid is proposed to minimize the cost of installing renewable energy resources (photovoltaic systems) as well as energy storage systems (batteries), in addition to the cost of operation over a long period of 20 years, which will include the cost of operating the power grid and the charging and discharging of the batteries.
- The full AC power flow constraints embedded into the long-term expansion planning framework ensure that all operating conditions are satisfied. Furthermore, it enables an accurate modeling for the loss as well as the voltage drop across the distribution network.
- To include all affecting parameters into the optimization process, the minimization is computed in accordance with the years (y), seasons (s), days of the week (d), time of the day (t), and different scenarios based on the usage of energy and its production (c).
- The difference between a centralized battery technology, e.g., RFB and decentralized technology, e.g., Li-ion battery is investigated in this work to compare and showcase the economic profits of these battery technologies.
- An IEEE 33-bus balanced distribution test bench is utilized in this work to evaluate the performance, effectiveness, and reliability of the proposed optimization and forecasting model.

The rest of this paper is organized as follows. In Section 2, the formulas for the optimization problem are derived. The solution method is presented in this section. In Section 3, the proposed optimization algorithm is implemented on an IEEE 33-bus balanced distribution test bench and the numerical results are presented. The discussion and analysis of obtained numerical results are then provided in Section 4. Finally, conclusions are drawn in Section 5.

2. Problem Formulation and Methodology

Consider a radial power grid network with *i* buses existing in the distribution grid as expressed in IEEE's 33-bus balanced distribution test system. A radial network is a tree shaped network with child, ch_i and ancestor A_i nodes connected to the *i*th node, such that there are no closed loops within the system that would lead to the origin. Due to the assumption of the existence of renewable energy resources on random buses, it can be assumed that any of these networks might be forced to operate in an islanded mode

due to reasons such as improving the reliability of the grid or preparing for unforeseen natural weather occurrences [33]. Subscript i denotes the number of buses on the network. Subscript SP denotes a specific solar panel on a bus, while subscripts B_L and B_F would denote specific Li-ion and RFB on each bus, respectively. The existence of each of these resources or energy systems on a specific bus is indicated by the Incident Matrix, A. Incident Matrices A_{SP}, A_{BL}, A_{BF}, and A_G represent the existence and the location of solar panels, Li-ion batteries, RFBs, and other power resources on the grid, respectively.

As mentioned earlier, the focus of this work is on planning and optimizing a long term expansion for a network, utilizing photo voltaic (PV) panels as well as battery storage resources. This expansion depends on the number of years, y, which would divide the market into one year time slots such that $y = 1; \ldots; Y$, where $Y = 20$. In addition, it would depend on the seasons of each year, s, where $s = 1; 2; 3; 4$; such that 1, 2, 3, and 4 represent Spring, Summer, Fall, and Winter, respectively. Moreover, the days of the week are also considered in this work in order to signify the difference between weekdays and weekends on the energy usage; therefore, the subscript d would either be 1 or 2 where 1 indicate weekdays and 2 represents weekends. The day-ahead energy market is also divided into 24 time slots, such that t ranges from 1 to 24. Other factors considered in the optimization are the 10 different demand scenarios, c, based on the usage of energy and its production, which also reflects the time of use (TOU) regulations set by the utility grid.

To minimize the cost of installation, maintenance, and operation of renewable energy resources in tandem with battery storage units, the objective function, $\mathscr{F}$, can be expressed as

$$
\mathscr{F} = Min\left(\left(\sum_y \sum_j \sum_k \left(C_{k,y}^{ins,j} I_{k,y}^{ins,j}\right)\right) + \right.
$$
$$
\left. \left(\sum_c \rho^c \sum_y \sum_s \sum_d \sum_t \left(P_{y,s,d,t,c}^{Grid} C_{y,s,d,t,c}^{Grid}\right)\right)\right),
\tag{1}
$$

where j used in the first term can either be PV, BL, or BF, and index k is pv, bl, and bf referring to existing PV, Li-ion, and RFB systems, respectively. In general, the first term represents the cost of installing either solar panels or battery storage units in a certain year, and the second term represents the cost of delivering power to the grid. This objective function consists of 3 different variable types, including decision variables, binary variables, and constant parameters. In this equation, the costs of the solar panels and batteries are 1-dimensional arrays of 1×20 which includes the depreciation of dollar value as well as the installation cost of each of these systems [34–36]. The cost of the grid's operation is assumed to be a constant parameter, however, the size of this array depends on the number of hours in a year. The prices considered in this array are based on TOU rates from San Diego Gas and Electric (SDG&E) for different times of the day, days of the week, and seasons of the year [37]. The demand of the grid is based on multiple 24×10 matrices that indicate the demand based on TOU, different scenarios of usage pattern, as well as the different seasons of the year. The power delivered by the grid is a decision variable, indicated by the solver itself, and the installation indices are binary variables, meaning that they can either be 0 or 1. Due to the existence of these different variable types in the objective function as well as the constraints mentioned in the following sections, this becomes an SOCP problem.

The binary assumptions for installation indices are made such that the following constraints are satisfied:

$$
I_{pv,y}^{ins,PV} = I_{pv,y}^{PV} - I_{pv,y-1}^{PV},
\tag{2a}
$$

$$
I_{bl,y}^{ins,BL} = I_{bl,y}^{BL} - I_{bl,y-1}^{BL},
\tag{2b}
$$

$$
I_{bf,y}^{ins,BF} = I_{bf,y}^{BF} - I_{bf,y-1}^{BF},
\tag{2c}
$$

where indices *pv*, *bl*, and *bf* refer to specific existing PV, Li-ion, and RFB systems, respectively. In other words, the above-mentioned sub-equations indicate that the current values of installation indices depend on what they were the year before, such that if they are 0, they will indicate no installation, and if they are 1, they will indicate the installation and existence of their respective devices. In order to solve the aforementioned objective function, there are multiple constraints that need to be taken into account. The first constraint will be based on the active and reactive power flow in the power network.

The active power flow in the network can be formulated as follows,

$$\sum_i \sum_c \sum_y \sum_s \sum_d \sum_t P^{inj,i}_{y,s,d,t,c} = \sum_i \sum_c \sum_y \sum_s \sum_d \sum_t \Big(\sum_{pv} A^i_{pv} P^{PV}_{pv,y,s,d,t,c}$$
$$+ \sum_g A^i_g P^{Grid}_{g,y,s,d,t,c} + \sum_{bl} A^i_{bl} (P^{dis,BL}_{bl,y,s,d,t,c} - P^{ch,BL}_{bl,y,s,d,t,c}) +$$
$$\sum_{bf} A^i_{bf} (P^{dis,BF}_{bf,y,s,d,t,c} - P^{ch,BF}_{bf,y,s,d,t,c}) - P^{D,i}_{y,s,d,t,c} \Big),$$

where the first term depicts the active power injected in the *i*th node of the bus, which is equal to the sum of all the power exiting (subtraction) or entering (addition) the bus based on the different years, seasons, days, times, scenarios, as well as individual PVs and batteries. Index *g* represents different tiers of usage. In this equation, all of the variables are considered to be decision variables except the demand power and the incident matrices that were discussed previously. The second term indicates the power dispatched by certain solar panels; the third term indicates the power dispatch of the grid; the fourth and fifth terms represent the power dispatch of the batteries based on their charge or discharge mode, such that if the battery is discharging it is injecting energy into the grid and when it is charging it is draining energy from the grid; and finally the sixth term indicates the demand power used by the costumers.

Similarly, the reactive power injection into the grid is formulated as follows,

$$\sum_i \sum_c \sum_y \sum_s \sum_d \sum_t Q^{inj,i}_{y,s,d,t,c} = \sum_i \sum_c \sum_y \sum_s \sum_d \sum_t \Big(\sum_{pv} A^i_{pv} Q^{inv,PV}_{pv,y,s,d,t,c}$$
$$+ \sum_g A^i_g Q^{Grid}_{g,y,s,d,t,c} + \sum_{bl} A^i_{bl} Q^{inv,BL}_{bl,y,s,d,t,c}$$
$$+ \sum_{bf} A^i_{bf} Q^{inv,BF}_{bf,y,s,d,t,c} - Q^{D,i}_{y,s,d,t,c} \Big),$$

where the reactive powers indicated in the first, third, and fourth terms are for the inverters of PVs, Li-ion batteries, and RFBs, respectively. Again, all of the variables in this equation are decision variables except the demand reactive power and the incident matrices.

The optimal power flow on each bus can also be modeled such that the dependence on the bus admittances, voltages, and phasors is evident. The set of Equations (3) through (5) formulate the AC active and reactive power flow equations and voltage bounds for each node. The active polar power flow equation is modeled as follows,

$$P^{inj,i} = GG_i v_i^2 + \sum_{j \in ch_i} \Big(GG_{i,j} v_i v_j \cos(\theta_i - \theta_j) - BB_{i,j} v_i v_j \sin(\theta_i - \theta_j) \Big)$$
$$+ GG_{i,a_i} v_i v_{ai} \cos(\theta_i - \theta_{a_i}) - BB_{i,a_i} v_i v_{ai} \sin(\theta_i - \theta_{a_i}), \tag{3}$$

in which the admittance values will be obtained from the IEEE 33-bus balanced distribution test systems [38,39]. The reactive polar power flow equation is similarly modeled as follows,

$$Q^{inj,i} = -BB_i v_i^2 + \sum_{j \in ch_i} -\Big(BB_{i,j} v_i v_j \cos(\theta_i - \theta_j) + GG_{i,j} v_i v_j \sin(\theta_i - \theta_j) \Big)$$
$$- BB_{i,a_i} v_i v_{ai} \cos(\theta_i - \theta_{a_i}) - GG_{i,a_i} v_i v_{ai} \sin(\theta_i - \theta_{a_i}), \tag{4}$$

such that

$$(Q^{inj,1})^2 + (P^{inj,1})^2 \leq (S_{tr})^2, \tag{5}$$

where S_{tr} is the capacity of the transformer connected to the first bus, and is assumed to be at $5MVA$. This value will be changed to $1MVA$ and $15MVA$ to evaluate the effect of the sizing of the distribution transformer on the bus. The voltage constraints for the ith node can be modeled as follows,

$$(V_i^{min})^2 \leq v_i^2 \leq (V_i^{max})^2, \tag{6}$$

where the limits on the voltage of the power delivered by utilities are enforced in the square form imposing a contract between the utility and the consumers to deliver the voltage within a limit which is usually 5% of the nominal value. In (6), V_i^{min} and V_i^{max} are the lower and upper limits for v_i, respectively, and are constant parameters, however, v_i itself is a decision variable. It should be noted that as both upper and lower limits are non-negative, enforcing the square form of the constraints will have the same impact as the one without squaring the limits and the voltage variable. Equation (6) can also be applied to the children and ancestor nodes of i as well. The main benefits of the AC power flow compared to the DC power flow or linearized AC power flow is the possibility of showing the voltages at each bus of the network. The limitations on the *sine* and *cosine* functions and phases are as follows,

$$\sum_i \theta_{i,a_i,ch_i} = 2\pi k, for\ some\ k\varepsilon\mathbb{Z}, \tag{7}$$

which indicates that the phase difference can range from zero (0) to any multiple of 2π.

Based on the constraints provided, it can be concluded that the current power flow model is a polar one, and therefore, hard to solve. To alleviate the extensive calculations and achieve higher computation efficiency, the rectangular and relaxed power flow models will be obtained later in this section.

The constraints of the power generated by each specific PV in the grid, *pv*, can be formulated as follows,

$$0 \leq P_{pv,y,s,d,t,c}^{PV} \leq I_{pv,y}^{PV} \times P_{pv,y,s,d,t,c}^{PV,max} \tag{8a}$$

$$I_{pv,y}^{PV} \geq I_{pv,y-1}^{PV} \tag{8b}$$

where (8a) states that the power generated by the PVs in the grid will always be less than that of the power capacity of the grid, which can be obtained by multiplying the existence variable of the PV by the total capacity of each panel based on the solar panel itself, year, season, day, time, and scenario.

The restrictions on the grid power are as follows,

$$0 \leq P_{g,y,s,d,t,c}^{Grid}, \tag{9a}$$

$$\rho^c (P_{g,y,s,weekday,t,c}^{Grid} \times 22 + P_{g,y,s,weekend,t,c}^{Grid} \times 8) \leq P_{g,y,s}^{Grid,max} \tag{9b}$$

where it can be seen from Equation (9a) that the power generated by the grid can never be negative and its lower bound is zero. Equation (9b) indicates the effect of the days of the week (weekday vs. weekend) on the power flowing in the grid. Based on these two restrictions, it can be concluded that the total power of the grid, considering the effect of the 10 different usage scenarios, and the days of the week will be restricted by the maximum capacity of the grid which is set by the scenario with the highest grid demand.

The reactive power restrictions for the PVs, RFBs, and Li-ion batteries are summarized as follows,

$$-Q_{pv}^{inv,PV,max} \times I_{pv,y}^{PV} \leq Q_{pv,y,s,d,t,c}^{inv,PV} \leq Q_{pv}^{inv,PV,max} \times I_{pv,y}^{PV} \tag{10}$$

$$-Q_{bl}^{inv,BL,max} \times I_{bl,y}^{BL} \leq Q_{bl,y,s,d,t,c}^{inv,BL} \leq Q_{bl}^{inv,BL,max} \times I_{bl,y}^{BL} \tag{11}$$

$$-Q_{bf}^{inv,BF,max} \times I_{bf,y}^{BF} \leq Q_{bf,y,s,d,t,c}^{inv,BF} \leq Q_{bf}^{inv,BF,max} \times I_{bf,y}^{BF} \tag{12}$$

Equations (10)–(12) indicate that the reactive power of the device needs to be restricted by the absolute value of the capacity of the inverters based on the existence variables. Again, it is worth to mention that the capacity variables are all constant parameters and the existence variables are all binary.

Since the contribution of this work is on distinguishing the difference between Li-ion batteries and RFBs in a long term expansion planning, the constraints and limitations on these two batteries are also formulated. The limitations on the Li-ion battery are as follows,

$$E_{bl,y,s,d,t,c}^{BL} = E_{bl,y,s,d,t-1,c}^{BL} + P_{bl,y,s,d,t,c}^{ch,BL} \times \eta_{BL} - \frac{P_{bl,y,s,d,t,c}^{dis,BL}}{\eta_{BL}} \tag{13}$$

$$E_{bl,y,s,d,0,c}^{BL} = E_{bl,y,s,d,24,c}^{BL} \tag{14}$$

$$E_{bl}^{BL,min} \times I_{bl,y}^{BL} \leq E_{bl,y,s,d,t-1,c}^{BL} \leq E_{bl}^{BL,max} \times (I_{bl,y}^{BL} - \sum_{y'}^{y} \alpha_{BL} I_{bl,y'}^{BL}) \tag{15}$$

$$0 \leq P_{bl,y,s,d,t,c}^{ch,BL} \leq P_{bl}^{ch,BL,max} \tag{16}$$

$$0 \leq P_{bl,y,s,d,t,c}^{dis,BL} \leq P_{bl}^{dis,BL,max} \tag{17}$$

$$0 \leq E_{bl,y,s,d,t,c}^{ch,BL} \leq E_{bl}^{BL,max} \times (I_{bl,y}^{BL} - \sum_{y'}^{y} \alpha_{BL} I_{bl,y'}^{BL}) \tag{18}$$

$$0 \leq E_{bl,y,s,d,t,c}^{dis,BL} \leq E_{bl}^{BL,max} \times (I_{bl,y}^{BL} - \sum_{y'}^{y} \alpha_{BL} I_{bl,y'}^{BL}) \tag{19}$$

Similarly, the limitations on the RFB are as follows,

$$E_{bf,y,s,d,t,c}^{BF} = E_{bf,y,s,d,t-1,c}^{BF} + P_{bf,y,s,d,t,c}^{ch,BF} \times \eta_{BF} - \frac{P_{bf,y,s,d,t,c}^{dis,BF}}{\eta_{BF}} \tag{20}$$

$$E_{bf,y,s,d,0,c}^{BF} = E_{bf,y,s,d,24,c}^{BF} \tag{21}$$

$$E_{bf}^{BF,min} \times I_{bf,y}^{BF} \leq E_{bf,y,s,d,t-1,c}^{BF} \leq E_{bf}^{BF,max} \times (I_{bf,y}^{BF} - \sum_{y'}^{y} \alpha_{BF} I_{bf,y'}^{BF}) \tag{22}$$

$$0 \leq P_{bf,y,s,d,t,c}^{ch,BF} \leq P_{bf}^{ch,BF,max} \tag{23}$$

$$0 \leq P_{bf,y,s,d,t,c}^{dis,BF} \leq P_{bf}^{dis,BF,max} \tag{24}$$

$$0 \leq E_{bf,y,s,d,t,c}^{ch,BF} \leq E_{bf}^{BF,max} \times (I_{bf,y}^{BF} - \sum_{y'}^{y} \alpha_{BF} I_{bf,y'}^{BF}) \tag{25}$$

$$0 \leq E_{bf,y,s,d,t,c}^{dis,BF} \leq E_{bf}^{BF,max} \times \left(I_{bf,y}^{BF} - \sum_{y'}^{y} \alpha_{BF} I_{bf,y'}^{BF}\right) \tag{26}$$

Equations (13) and (20) refer to the energy available in the battery unit. In other words, they are referring to the condition which states that the energy stored in the battery at the current time t depends on its energy at $t-1$ in addition to the energy consumed during charging of the battery and the energy extracted from the node based on the discharge of the battery. Equations (14) and (21) refer to the fact that the energy stored in the battery at the end of the day has to be equal to its value at the beginning of the day. Equations (15) and (22) formulate the limitations on the dispatch of the battery units based on their installation indices. Equations (16)–(19) and (23)–(26) refer to the constraints on the charge and discharge energy dispatch of the batteries. The last term in (18) and (19) presents the impact of battery aging on its charging and discharge rate. The maximum capacity variables in all Equations (13) through (26), as well as the efficiency factors are constant parameters. The charging and discharging efficiencies are considered to be the same for both RFB and Li-ion battery. The charge and discharge powers as well as battery capacities are decision variables, and the existence variables are binary values in these equations.

As it was mentioned earlier, it can be seen that the problem is in the form of a nonconvex nonlinear optimization problem. The reason for this is the nonlinearity of the bus voltages and their corresponding phase differences as demonstrated in (3)–(5). Another reason is due to the quadratic constraints on the voltage limitations, as formulated in (6). Nonlinear functions are amongst the hardest and most complicated to solve and optimize, and therefore, need to somehow be simplified in order to become solvable. That is why the aforementioned equations are convexified and the problem is converted to an SOCP relaxation operation problem.

To this end, the nonconvex and nonlinear power flow and constraint equations, which we have previously derived, are relaxed using the methods presented in [31]. Initially, these equations need to be transformed from the polar environment to the rectangular environment, such that the power flow equations transforms as follows,

$$
\begin{aligned}
P^{inj,i} = {}& GG_i(e_i^2 + f_i^2) + \sum_{j \in ch_i} GG_{i,j}(e_i e_j + f_i f_j) - BB_{i,j}(e_i f_j - f_i e_j) \\
& + GG_{i,a_i}(e_i e_{a_i} + f_i f_{a_i}) - BB_{i,a_i}(e_i f_{a_i} - f_i e_{a_i}),
\end{aligned}
\tag{27}
$$

$$
\begin{aligned}
Q^{inj,i} = {}& -\Big(BB_i(e_i^2 + f_i^2) + \sum_{j \in ch_i} BB_{i,j}(e_i e_j + f_i f_j) + GG_{i,j}(e_i f_j - f_i e_j) \\
& + BB_{i,a_i}(e_i e_{a_i} + f_i f_{a_i}) + GG_{i,a_i}(e_i f_{a_i} - f_i e_{a_i}), \Big)
\end{aligned}
\tag{28}
$$

where (27) represents the active rectangular power flow model and (28) represents the reactive rectangular power flow model. It can be seen that even the rectangular model has some quadratic terms which leads to a lengthy optimization process. The relaxed optimal power flow model would require the following substitutions for the e_i and f_i terms:

$$
\begin{aligned}
e_i^2 + f_i^2 &= cc_{ii}, \\
e_i e_{ch_i} + f_i f_{ch_i} &= cc_{i,ch_i}, \\
e_i e_{a_i} + f_i f_{a_i} &= cc_{i,a_i}, \\
e_i f_{ch_i} - f_i e_{ch_i} &= ss_{i,ch_i}, \\
e_i f_{a_i} - f_i e_{a_i} &= ss_{i,a_i}.
\end{aligned}
\tag{29}
$$

As it can be seen, all of the previous quadratic terms are now replaced by linear terms, which will be substituted in the power flow equation to obtain the semi-relaxed model.

$$P^{inj,i} = GG_i cc_{ii} + \sum_{j \in ch_i} \left(GG_{i,j} cc_{i,j} - BB_{i,j} ss_{i,j} \right) + GG_{i,a_i} cc_{i,a_i} - BB_{i,a_i} ss_{i,a_i}, \tag{30}$$

$$Q^{inj,i} = -\left(BB_i cc_{ii} + \sum_{j \in ch_i} (BB_{i,j} cc_{i,j} + GG_{i,j} ss_{i,j}) + BB_{i,a_i} cc_{i,a_i} + GG_{i,a_i} ss_{i,a_i} \right), \tag{31}$$

where (30) represents the semi-relaxed active power flow model and (31) represents the semi-relaxed reactive power flow model. Here, the real and imaginary bus admittance is extracted from the IEEE 33-bus balanced distribution test system. The constraints on these decision variables are defined as follows,

$$\begin{aligned}
cc_{i,ch_i}{}^2 + ss_{i,ch_i}{}^2 &\leq cc_{ii} cc_{ch_i,ch_i}, \\
cc_{i,a_i}{}^2 + ss_{i,a_i}{}^2 &\leq cc_{ii} cc_{a_i,a_i}, \\
cc_{i,ch_i} &= cc_{ch_i,i}, \\
cc_{i,a_i} &= cc_{a_i,i}, \\
ss_{i,ch_i} &= -ss_{ch_i,i}, \\
ss_{i,a_i} &= -ss_{a_i,i}.
\end{aligned} \tag{32}$$

The conditions that transforms this model from a semi-relaxed to a completely relaxed model are the first and second terms in (32).

Essentially, the two variables cc and ss are replacing the voltage and phase terms, therefore, the constraints on the voltage with respect to the variables will be transformed to:

$$(V_i^{min})^2 \leq cc_{ii} \leq (V_i^{max})^2, \tag{33}$$

and the voltages of the bus components could then be defined and obtained as follows,

$$\begin{aligned}
cc_{i,ch_i}{}^2 &= v_i v_{ch_i} \cos(\theta_i - \theta_{ch_i}), \\
cc_{i,a_i}{}^2 &= v_i v_{a_i} \cos(\theta_i - \theta_{a_i}), \\
ss_{i,ch_i}{}^2 &= v_i v_{ch_i} \sin(\theta_i - \theta_{ch_i}), \\
ss_{i,a_i}{}^2 &= v_i a_{a_i} \sin(\theta_i - \theta_{a_i}).
\end{aligned} \tag{34}$$

where cc, ss, phasors, and voltages are decision variables defined without initialization, and are obtained based on the objective function. The capacity or maximum values in these equations are the only variables that are defined as constant parameters. It can be seen that the proposed relaxation strategy does not have any nonlinear and quadratic terms, and is relaxed for modeling.

3. Numerical Results

The power flow, battery storage, and constraint formulations are modeled in the YALMIP environment [40] and solved using the Gurobi solver [41]. The solver is run on an HP Pavilion g6 Notebook PC with 4 GB memory. The IEEE 33-bus balanced distribution test bench is also used as an input for the model alongside the incident matrices, cost vectors, and constant parameters. The constant parameters for the demand and rates were obtained from [37], the battery, and solar panel information, including the inverter sizes as well as their capacity were obtained from [42–48]. These values are summarized in Tables 1–6. In order to assess the benefits of employing renewable energy resources as well as energy storage units, multiple scenarios are considered and analyzed.

Multiple scenarios are considered in this work. Some scenarios are based on the capacity and number of buses that are occupied by solar panels and Li-ion batteries. Other scenarios consider the size of the transformer at the distribution bus. In addition, we

considered a specific scenario that shows how efficient the system would be with only Li-ion or RFB present. The results for the percentage of loss, voltage profile, and optimal cost of each scenario are shown in Figures 1–3, and are summarized in Table 7 for different scenarios that are briefly explained below:

- **Scenario I:** This scenario considers close to minimum number of PVs and Li-ion batteries (on 4 buses only) with a transformer size of $5MVA$. In addition, RFB has been connected to the first bus of the grid. This scenario is chosen as a basis for the voltage profile comparison of different scenarios.
- **Scenario II:** This scenario considers the situation where half of the buses of the network have PVs and Li-ion batteries installed (16 buses only) with a transformer size of $5MVA$. In addition, RFB has been connected to the first bus of the grid.
- **Scenario III:** This scenario considers the situation where almost all of the buses of the network have PVs and Li-ion batteries installed (32 buses only) with a transformer size of $5MVA$. In addition, RFB has been connected to the first bus of the grid.
- **Scenario IV:** This scenario considers the existence of the PVs (on 4 buses only) and RFB connected to the first bus of the grid, however, eliminates any Li-ion batteries in order to assess their effect on the network. The transformer is considered to be $5MVA$.
- **Scenario V:** This scenario considers the existence of the PVs and the Li-ion batteries (on 4 buses only); however, it eliminates any RFB in order to assess their effect on the network. The transformer considered is $5MVA$.
- **Scenario VI:** This scenario considers a distribution transformer of size $15MVA$. This system has PVs and Li-ion batteries on 4 buses and the RFB on the first bus of the grid.
- **Scenario VII:** This scenario considers a distribution transformer of size $1MVA$. This system has PVs and Li-ion batteries on 4 buses and the RFB on the first bus of the grid.

Table 1. Effective lower and upper bounds for RFB (capacity of 6000 kWh and SOC range of 5% to 95%) and Li-ion battery (capacity of 300 kWh with SOC range of 15% to 85%).

System Type	Min. Capacity (kWh)	Max. Capacity (kWh)
Li-ion Battery	45	255
RFB	300	5700

Table 2. Charging and discharging power rating for RFB (capacity of 6000 kWh with SOC range of 5% to 95%) and Li-ion (capacity of 300 kWh with SOC range of 15% to 85%).

System Type	Maximum Charging Power (kW)	Maximum Discharging Power (kW)
Li-ion Battery	−8	50
RFB	−60	1200

Table 3. Maximum power production of the grid and PV.

System Type	Maximum Power (kW)
Grid	5000
PV	150

Table 4. Inverter capacity for PV, RFB, and Li-ion battery.

System Type	Capacity (KVA)
PV Inverter	150
Li-ion Battery Inverter	300
RFB Inverter	6000

Table 5. Efficiency and degradation factors (%).

Factors	α_{BF}	η_{BF}	α_{BL}	η_{BL}	ρ^c
Numerical Value (%)	0.96	0.9	0.9	0.95	0.1

Table 6. Installation costs for the solar panels (cost depreciation factor of 2.5%), Li-ion batteries (cost depreciation factor of 4%), and RFB (cost depreciation factor of 4%) in ($/kWh) over the span of 20 years.

Year	PV Cost ($/kWh)	Li-ion Battery Cost ($/kWh)	RFB Cost ($/kWh)
1	250	273	500
2	243.75	262.08	480
3	237.66	251.6	460.8
4	231.71	241.53	442.37
5	225.92	231.87	424.67
6	220.27	222.6	407.69
7	214.77	213.69	391.38
8	209.4	205.15	375.72
9	204.16	196.94	360.69
10	199.06	189.06	346.27
11	194.08	181.5	332.42
12	189.23	174.24	319.12
13	184.5	167.27	306.35
14	180.32	161.42	294.1
15	176.71	155.77	282.33
16	173.18	150.31	271.34
17	169.72	145.05	260.2
18	166.32	139.98	249.79
19	162.99	135.08	239.8
20	159.74	130.35	230.21

Table 7. Optimal cost and power loss for different scenarios.

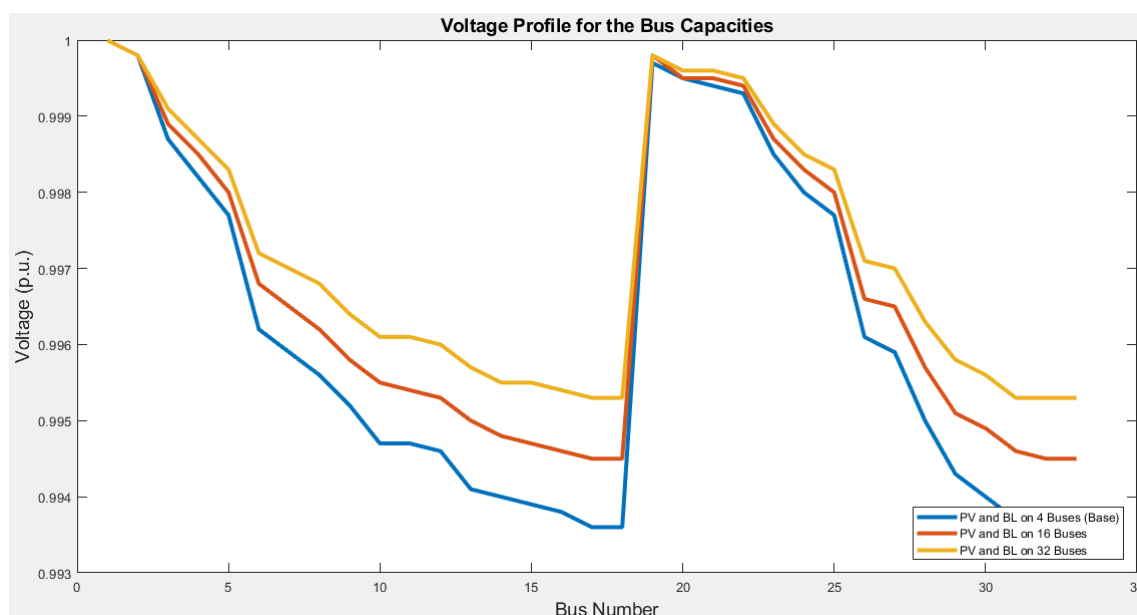| Scenarios	Power Loss (%)	Optimal Cost ($)
I	0.51158	14,179,000
II	0.49336	17,505,000
III	0.36438	18,940,000
IV	0.42369	12,194,000
V	0.5233	10,804,000
VI	0.82162	22,728,000
VII	0.48341	13,441,000

Figure 1. The grid's voltage profile for different penetration levels of PV and battery storage (both Li-ion and RFB) systems: Scenario I with low penetration level (only on 4 buses), Scenario II with medium penetration level (16 buses), and Scenario III with high penetration level (32 buses).
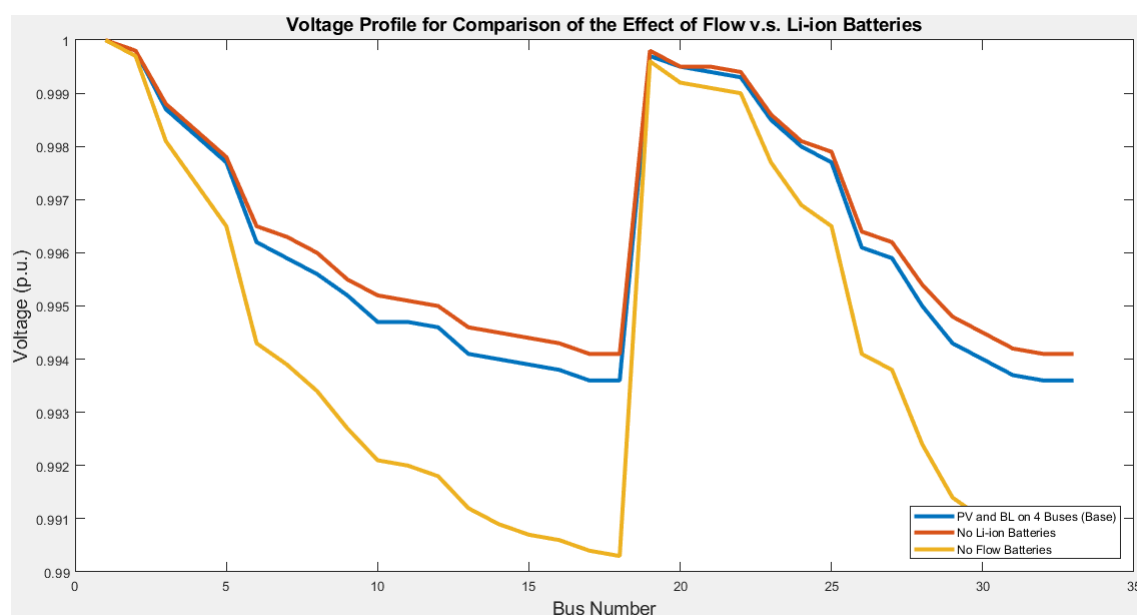

Figure 2. The grid's voltage profile for different battery storage technologies, i.e., Li-ion battery and RFB: Scenario I with both Li-ion batteries and RFB, Scenario IV with only RFB and no Li-ion batteries, and Scenario V with only Li-ion batteries and no RFB.
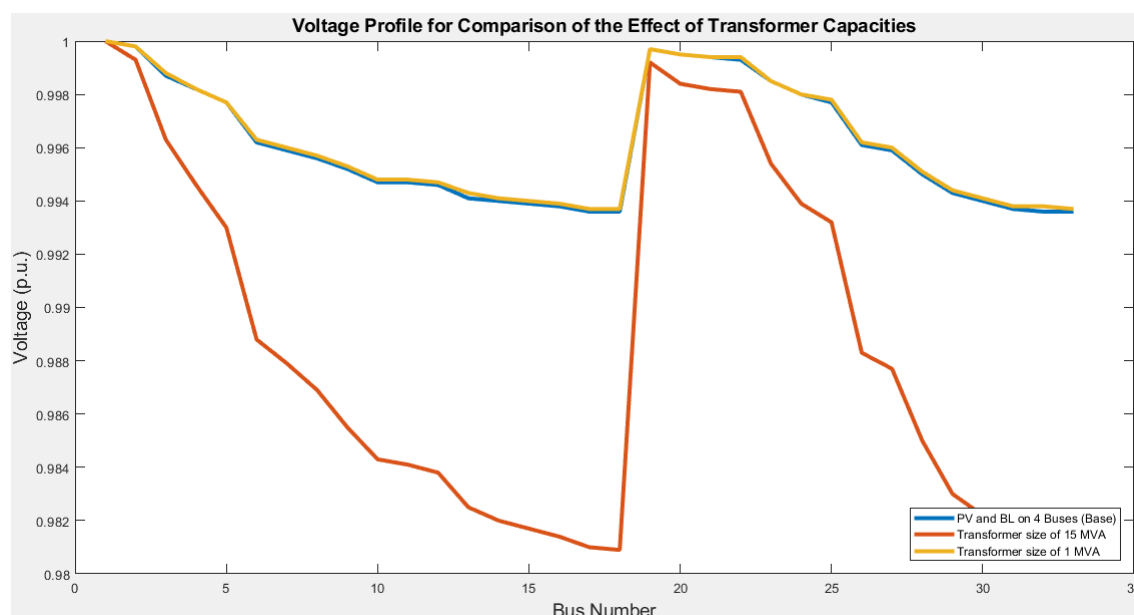
Figure 3. The grid's voltage profile for different sizes of distribution transformer: Scenario I with a 5*MVA* transformer, Scenario VI with a 15*MVA* transformer, and Scenario VII with a 1*MVA* transformer.

4. Analysis and Discussion

Comparing the results of all the investigated scenarios, it is evident that the grid's voltage profile is improved with high penetration level of PVs and battery storage systems as shown in Figure 1. In addition, it is discernible that the efficiency of the grid is best when RFBs are employed. Furthermore, Figure 2 showcases that the voltage profile of the system is much improved with RFBs compared to scenarios where no RFBs are employed. It is also observed from Figure 3 that increasing the capacity of distribution transformer will deteriorate the grid's voltage profile. It should be noted that in all figures, the voltage-drop happening on the 18th bus is due to the topology of the grid, where the 18th bus is the last bus on the grid and it would experience the least voltage due to transmission losses [49]. It can be seen that the best option in terms of capacity for the grid is Scenario III where almost all the buses (32 buses out of 33) have installed PV and both Li-ion batteries and RFB, since the loss percentage is the lowest among all scenarios as summarized in Table 7. Figure 1 also confirms this hypothesis since it shows that voltage deviation is lowest for this scenario. It should be noted that in Scenario III, the first bus is only connected to RFB. If the first bus is also populated with PVs, Li-ion batteries, or both, the model becomes unstable. That might be due to the additional load that each PV or Li-ion battery, especially in charging phase, adds to each bus. Therefore, an imbalance in the load on the first bus might be the reason for the instability of the system with all buses equipped with PVs and Li-ion batteries.

It was demonstrated that if the power network is not employing RFBs (Scenario V), while the total operation and maintenance cost is lower, the efficiency of the network is decreased and the voltage is not regulated, as shown in Figure 2. In terms of transformer capacity, it can be seen that if RFBs are employed, a smaller size transformer is both cost and energy efficient (Scenario VII), compared to utilizing a larger one (Scenario VI). This is also evident from Figure 3 illustrating that the smaller transformer has less deviation from the base case (Scenario I). In fact utilizing a larger distribution transformer (Scenario VI) is the least cost and energy efficient case among all scenarios. This research demonstrates the effectiveness of RFBs compared to Li-ion in regulating the voltage of the distribution power network as well as increasing the efficiency of the distribution grid. The results also show that with the current price trends for the installment of energy storage systems, addition of the Li-ion batteries combined with PVs on a selected number of buses is the least expensive solution for a sustainable distribution grid powered with renewable energy

resources. Therefore, the immediate installation of a small number of Li-ion batteries across several buses within the distribution network is the optimal expansion planning strategy. In addition, comparing Li-ion and RFB storage technologies, on balance, Li-ion technology is a better choice for the electricity distribution network.

5. Conclusions

This paper proposed a long-term expansion and optimization framework for the smart distribution network to investigate long-term efficiency of Li-ion and RFBs in terms of economics for the customers as well as the operating utility company. The formulation used for the power flow as well as the constraints considered an SOCP algorithm, and the model was linearized by applying the relaxed AC optimal power flow (ACOPF) model. These algorithms were implemented on an IEEE 33-bus balanced distribution testbed system. The proposed optimization algorithm was tested in several different scenarios to investigate the effects of penetration level of PVs, RFB and Li-ion battery storage technologies as well as the capacity of the distribution transformer. The results demonstrate the efficiency and effectiveness of the proposed optimization model, revealing that installing Li-ion batteries on several buses of the distribution network is the optimal expansion planning strategy.

Abbreviations

The following abbreviations are used in this manuscript:

BESS	Battery energy storage system
ESS	Energy storage system
Li-ion	Lithium-ion
RFB	Redox flow battery
SOCP	Second order cone programming
ACOPF	AC optimal power flow
TOU	Time of use
PV	Photovoltaic
GHG	Green house gas
SDG&E	San Diego Gas and Electric
DOE	Department oF Energy

Nomenclature

A^i	Incident matrix on node i
P^{PV}	Active power of PV
p^{Grid}	Active power of the grid
$p^{ch,BL}$	Active power of charging Li-ion battery
$p^{ch,BF}$	Active power of charging RFB
$p^{dis,BL}$	Active power of discharging Li-ion battery
$p^{dis,BF}$	Active power of discharging RFB battery
P^D	Active power of demand
P^{inj}	Injected active power
Q^{Grid}	Reactive power of the grid
Q^D	Reactive power of demand
Q^{inj}	Injected reactive power

$C^{ins,PV}$	PV installation Cost
$C^{ins,BL}$	Li-ion installation Cost
$C^{ins,BF}$	RFB installation Cost
C^{Grid}	Cost of power from the grid at different tiers of energy usage
$I^{ins,PV}$	Decision index of installing PV
I^{PV}	Existence variable of PV
$I^{ins,BL}$	Decision index of installing Li-ion battery
I^{BL}	Existence variable of Li-ion battery
$I^{ins,BF}$	Decision index of installing RFB
I^{BF}	Existence variable of RFB
ρ^c	Probability factor of the occurrence of each scenario
BB_i	Susceptance of the line connecting to node i
GG_i	Conductance of line connecting to node i
v_i	Voltage of node i
v_{ch_i}	Voltage of node ch_i, the children nodes of i
v_{a_i}	Voltage of node a_i, the ancestor nodes of i
V_i^{min}	Minimum voltage of node i
V_i^{max}	Maximum voltage of node i
e_i	The real part of voltage phasor of node i
e_{ch_i}	The real part of voltage phasor of node ch_i, the children nodes of i
e_{a_i}	The real part of voltage phasor of node a_i, the ancestor nodes of i
f_i	The imaginary part of voltage phasor of node i
f_{ch_i}	The imaginary part of voltage phasor of node ch_i, the children nodes of i
f_{a_i}	The imaginary part of voltage phasor of node a_i, the ancestor nodes of i
$cc_{i,i}$	The lifting variable associated with node i
cc_{i,ch_i}	The lifting variable associated with node i and its children nodes ch_i
cc_{i,a_i}	The lifting variable associated with node i and its ancestor nodes a_i
$ss_{i,i}$	The lifting variable associated with node i
ss_{i,ch_i}	The lifting variable associated with node i and its children nodes ch_i
ss_{i,a_i}	The lifting variable associated with node i and its ancestor nodes a_i
θ_i	Phase of node i
θ_{ch_i}	Phase of node ch_i, the children nodes of i
θ_{a_i}	Phase of node a_i, the ancestor nodes of i
$P^{PV,max}$	Power production capacity of the PV
$P^{Grid,max}$	Power production capacity of the grid
$Q^{inv,PV}$	Reactive power of the PV inverter
$Q^{inv,BL}$	Reactive power of the Li-ion battery inverter
$Q^{inv,BF}$	Reactive power of the RFB inverter
$Q^{inv,PV,max}$	Reactive power capacity of the PV inverter
$Q^{inv,BL,max}$	Reactive power capacity of the Li-ion battery inverter
$Q^{inv,BF,max}$	Reactive power capacity of the RFB inverter
E^{BL}	Energy stored in Li-ion battery
E^{BF}	Energy stored in RFB
$E^{ch,BL}$	Charging energy of Li-ion battery
$E^{dis,BL}$	Discharging energy of Li-ion battery
$E^{ch,BF}$	Charging energy of RFB
$E^{dis,BF}$	Discharging energy of RFB
$E^{BL,min}$	Minimum energy stored in Li-ion battery
$E^{BL,max}$	Maximum energy stored in Li-ion battery
$E^{BF,min}$	Minimum energy stored in RFB
$E^{BF,max}$	Maximum energy stored in RFB
α_{BL}	Degradation of Li-ion battery
α_{BF}	Degradation of RFB
η_{BL}	Efficiency of Li-ion battery
η_{BF}	Efficiency of RFB
S_{tr}	Transformer capacity

References

1. Kanchev, H.; Lu, D.; Colas, F.; Lazarov, V.; Francois, B. Energy management and operational planning of a microgrid with a PV-based active generator for smart grid applications. *IEEE Trans. Ind. Electron.* **2011**, *58*, 4583–4592. [CrossRef]
2. Chen, C.; Duan, S.; Cai, T.; Liu, B.; Hu, G. Smart energy management system for optimal microgrid economic operation. *IET Renew. Power Gener.* **2011**, *5*, 258–267. [CrossRef]
3. Durrani, S.P.; Balluff, S.; Wurzer, L.; Krauter, S. Photovoltaic yield prediction using an irradiance forecast model based on multiple neural networks. *J. Mod. Power Syst. Clean Energy* **2018**, *6*, 255–267. [CrossRef]
4. Atwa, Y.; El-Saadany, E.; Salama, M.; Seethapathy, R. Optimal renewable resources mix for distribution system energy loss minimization. *IEEE Trans. Power Syst.* **2010**, *25*, 360–370. [CrossRef]
5. Qiu, X.; Nguyen, T.A.; Guggenberger, J.D.; Crow, M.L.; Elmore, A.C. A Field Validated Model of a Vanadium Redox Flow Battery for Microgrids. *IEEE Trans. Smart Grid* **2014**, *5*, 1592–1601. [CrossRef]
6. Department of Energy: Smart Grid. Available online: https://www.energy.gov/science-innovation/electric-power/smart-grid (accessed on 1 October 2019).
7. Latifi, M.; Sabzehgar, R.; Fajri, P.; Rasouli, M. A Novel Control Strategy for the Frequency and Voltage Regulation of Distribution Grids Using Electric Vehicle Batteries. *Energies* **2021**, *14*, 1435. [CrossRef]
8. Sabzehgar, R.; Kazemi, M.; Rasouli, M.; Fajri, P. Cost optimization and reliability assessment of a microgrid with large-scale plug-in electric vehicles participating in demand response programs. *Int. J. Green Energy* **2020**, *17*, 127–136. [CrossRef]
9. Latifi, M.; Sabzehgar, R.; Rasouli, M.; Fajri, P. Active and reactive power compensation using a pev-based three-level capacitor clamped inverter. In Proceedings of the 2019 IEEE Texas Power and Energy Conference (TPEC), College Station, TX, USA, 7–8 February 2019; pp. 1–6.
10. Latifi, M.; Sabzehgar, R.; Rasouli, M. Reactive power compensation using plugged-in electric vehicles for an ac power grid. In Proceedings of the IECON 2018–44th Annual Conference of the IEEE Industrial Electronics Society, Washington, DC, USA, 21–23 October 2018; pp. 4986–4991.
11. Mohsenian-Rad, H. Coordinated price-maker operation of large energy storage units in nodal energy markets. *IEEE Trans. Power Syst.* **2016**, *31*, 786–797. [CrossRef]
12. Aznavi, S.; Fajri, P.; Sabzehgar, R.; Asrari, A. Optimal management of residential energy storage systems in presence of intermittencies. *J. Build. Eng.* **2020**, *29*, 101149. [CrossRef]
13. Kazemi, M.A.; Sabzehgar, R.; Rasouli, M. An optimized scheduling strategy for plugged-in electric vehicles integrated into a residential smart microgrid for both grid-tied and islanded modes. In Proceedings of the 2017 IEEE 6th International Conference on Renewable Energy Research and Applications (ICRERA), San Diego, CA, USA, 5–8 November 2017; pp. 251–256.
14. Lucas, A.; Chondrogiannis, S. Smart grid energy storage controller for frequency regulation and peak shaving, using a vanadium redox flow battery. *Int. J. Electr. Power Energy Syst.* **2016**, *80*, 26–36. [CrossRef]
15. Zimmerman, N. *Vanadium Redox Flow Battery: Sizing of VRB in Electrified Heavy Construction Equipment*; Vanadium Crop.: Vancouver, BC, Canada, 2014.
16. Uhrig, M.; Koenig, S.; Suriyah, M.R.; Leibfried, T. Lithium-based vs. Vanadium Redox Flow Batteries—A Comparison for Home Storage Systems. *Energy Procedia* **2016**, *99*, 35–43. [CrossRef]
17. Durmus, Y.E.; Zhang, H.; Baakes, F.; Desmaizieres, G.; Hayun, H.; Yang, L.; Kolek, M.; Küpers, V.; Janek, J.; Mandler, D.; et al. Side by Side Battery Technologies with Lithium-Ion Based Batteries. *Adv. Energy Mater.* **2020**, *10*, 2000089. [CrossRef]
18. Wang, Y.; He, P.; Zhou, H. Li-Redox Flow Batteries Based on Hybrid Electrolytes: At the Cross Road between Li-ion and Redox Flow Batteries. *Adv. Energy Mater.* **2012**, *2*, 770–779. [CrossRef]
19. Ehsan, A.; Yang, Q. Coordinated investment planning of distributed multi-type stochastic generation and battery storage in active distribution networks. *IEEE Trans. Sustain. Energy* **2018**, *10*, 1813–1822. [CrossRef]
20. Ha, S.; Gallagher, K.G. Estimating the system price of redox flow batteries for grid storage. *J. Power Source* **2015**, *296*, 122–132. [CrossRef]
21. Jiang, H.; Sun, J.; Wei, L.; Wu, M.; Shyy, W.; Zhao, T. A high power density and long cycle life vanadium redox flow battery. *Energy Storage Mater.* **2020**, *24*, 529–540. [CrossRef]
22. Chen, H.; Liu, Y.; Zhang, X.; Lan, Q.; Chu, Y.; Li, Y.; Wu, Q. Single-component slurry based lithium-ion flow battery with 3D current collectors. *J. Power Source* **2021**, *485*, 229319. [CrossRef]
23. Wang, X.; Chai, J.; Jiang, J. Redox flow batteries based on insoluble redox-active materials. A review. *Nano Mater. Sci.* **2021**, *3*, 17–24. [CrossRef]
24. Girschik, J.; Kopietz, L.; Joemann, M.; Grevé, A.; Doetsch, C. Redox flow batteries: Stationary energy storages with potential. *Chem. Ing. Tech.* **2021**, *93*, 523–533. [CrossRef]
25. Chen, S.; Gooi, H.B.; Wang, M. Sizing of energy storage for microgrids. *IEEE Trans. Smart Grid* **2012**, *3*, 142–151. [CrossRef]
26. Parvania, M.; Fotuhi-Firuzabad, M.; Shahidehpour, M. Comparative hourly scheduling of centralized and distributed storage in day-ahead markets. *IEEE Trans. Sustain. Energy* **2014**, *5*, 729–737. [CrossRef]
27. Goebel, C.; Cheng, V.; Jacobsen, H.A. Profitability of residential battery energy storage combined with solar photovoltaics. *Energies* **2017**, *10*, 976. [CrossRef]
28. Carroquino, J.; Roda, V.; Mustata, R.; Yago, J.; Valiño, L.; Lozano, A.; Barreras, F. Combined production of electricity and hydrogen from solar energy and its use in the wine sector. *Renew. Energy* **2018**, *122*, 251–263. [CrossRef]

29. Marczinkowski, H.M.; Østergaard, P.A. Residential versus communal combination of photovoltaic and battery in smart energy systems. *Energy* **2018**, *152*, 466–475. [CrossRef]

30. Gholami, A.; Sun, X.A. Towards resilient operation of multimicrogrids: An misocp-based frequency-constrained approach. *IEEE Trans. Control Netw. Syst.* **2018**, *6*, 925–936. [CrossRef]

31. Kocuk, B.; Dey, S.S.; Sun, X.A. Strong SOCP relaxations for the optimal power flow problem. *Oper. Res.* **2016**, *64*, 1177–1196. [CrossRef]

32. Farivar, M.; Low, S.H. Branch flow model: Relaxations and convexification—Part I. *IEEE Trans. Power Syst.* **2013**, *28*, 2554–2564. [CrossRef]

33. Photovoltaics, D.G.; Storage, E. *IEEE Standard for Interconnection and Interoperability of Distributed Energy Resources with Associated Electric Power Systems Interfaces*; IEEE: Piscataway, NJ, USA, 2018.

34. Kellogg, W.; Nehrir, M.; Venkataramanan, G.; Gerez, V. Generation unit sizing and cost analysis for stand-alone wind, photovoltaic, and hybrid wind/PV systems. *IEEE Trans. Energy Convers.* **1998**, *13*, 70–75. [CrossRef]

35. Lache, R.; Galves, D.; Nolan, P. *Electric Cars: Plugged in*; Prepared for the Autos Research Team; Deutsche Bank Securities Inc.: New York, NY, USA, 2008.

36. Viswanathan, V.; Crawford, A.; Stephenson, D.; Kim, S.; Wang, W.; Li, B.; Coffey, G.; Thomsen, E.; Graff, G.; Balducci, P.; et al. Cost and performance model for redox flow batteries. *J. Power Source* **2014**, *247*, 1040–1051. [CrossRef]

37. San Diego Gas & Electric (SDG&E). Available online: https://www.sdge.com (accessed on 1 October 2019).

38. Zimmerman, R.D.; Murillo-Sánchez, C.E.; Thomas, R.J. MATPOWER: Steady-state operations, planning, and analysis tools for power systems research and education. *IEEE Trans. Power Syst.* **2011**, *26*, 12–19. [CrossRef]

39. Murillo-Sánchez, C.E.; Zimmerman, R.D.; Anderson, C.L.; Thomas, R.J. Secure planning and operations of systems with stochastic sources, energy storage, and active demand. *IEEE Trans. Smart Grid* **2013**, *4*, 2220–2229. [CrossRef]

40. Löfberg, J. YALMIP: A toolbox for modeling and optimization in MATLAB. In Proceedings of the CACSD Conference, Taipei, Taiwan, 2–4 September 2004; Volume 3.

41. Gurobi Optimization Inc. *Gurobi Optimizer Reference Manual*; Gurobi Optimization Inc.: Beaverton, OR, USA, 2014.

42. Leadbetter, J. Residential Battery Energy Storage Systems for Renewable Energy Integration and Peak Shaving. Ph.D. Thesis, Dalhousie University, Halifax, NS, Canada, 2012.

43. Schaltz, E.; Khaligh, A.; Rasmussen, P.O. Influence of battery/ultracapacitor energy-storage sizing on battery lifetime in a fuel cell hybrid electric vehicle. *IEEE Trans. Veh. Technol.* **2009**, *58*, 3882–3891. [CrossRef]

44. Li, C.H.; Zhu, X.J.; Cao, G.Y.; Sui, S.; Hu, M.R. Dynamic modeling and sizing optimization of stand-alone photovoltaic power systems using hybrid energy storage technology. *Renew. Energy* **2009**, *34*, 815–826. [CrossRef]

45. Maity, I.; Rao, S. Simulation and pricing mechanism analysis of a solar-powered electrical microgrid. *IEEE Syst. J.* **2010**, *4*, 275–284. [CrossRef]

46. Demoulias, C. A new simple analytical method for calculating the optimum inverter size in grid-connected PV plants. *Electr. Power Syst. Res.* **2010**, *80*, 1197–1204. [CrossRef]

47. Burger, B.; Rüther, R. Inverter sizing of grid-connected photovoltaic systems in the light of local solar resource distribution characteristics and temperature. *Sol. Energy* **2006**, *80*, 32–45. [CrossRef]

48. Xiong, R.; He, H.; Sun, F.; Zhao, K. Online estimation of peak power capability of Li-ion batteries in electric vehicles by a hardware-in-loop approach. *Energies* **2012**, *5*, 1455–1469. [CrossRef]

49. Taher, S.A.; Afsari, S.A. Optimal location and sizing of UPQC in distribution networks using differential evolution algorithm. *Math. Probl. Eng.* **2012**, *2012*, 838629. [CrossRef]